Simulation Study of Voxel-Based Head Phantom for Medical Microwave Imaging

Mladjen Stevanetic, Branko Kolundzija, Tushar Singh, Marija Nikolic Stevanovic

Abstract—The paper describes the crucial role of phantoms in Microwave Imaging (MWI) for medical devices. Accurate modelling of numerical scenarios is crucial in designing, testing, and developing MWI devices. Phantoms with appropriate tissue electrical properties are inevitable components of imaging scenarios. Therefore, high computing resources are required to develop such phantom, and EM simulation of such scenarios requires a more prolonged time. A defined blueprint is required to reduce the complexity of such scenarios to use them effectively for MWI purposes. In the given paper, a brief study of the three-dimension voxel model of the head is presented, where a unit cell is a cube with tissue-mimicking properties. The phantom is developed on the WIPL-D Pro EM simulation platform. Further, the voxels are grouped in the form of N x N x N, where N is the number of voxels on each axis. Homogenization techniques are implemented on the grouped voxels and result in one big cube, the main building element of the electromagnetic model. The RCS simulation is performed with plane wave excitation for different values of N, and the results are analyzed for convergence to the reference model. Also, the relative mean absolute deviation (RMA) of the whole phantom as a result of the homogenization process is presented and its convergence is compared with the convergence of the mean deviation of simulated results.

Index Terms—Head phantom; Microwave Imaging; Voxel Model; Zubal

I. INTRODUCTION

BRAIN stroke has been one of the leading causes of death in humans over the last decade. Early-stage screening of stroke is a crucial step for diagnosis and treatment purposes [1]. Conventional technologies such as MRI, CT and X-ray are the gold standard for stroke detection due to accurate scanned results with high spatial resolution for clinical diagnosis. Although, these methods have several disadvantages, such as expensive procedures, low portability and ionizing radiation [2] – [3]. On the other hand, Microwave Imaging (MWI) is envisioned as a complementary tool to the imaging technologies for brain stroke detection. It is a low health risk, non-invasive, and cost-effective procedure [4] – [5].

Developing medical devices based on microwave imaging requires accurate electromagnetic modelling of imaging scenarios. The vital components of imaging scenarios are powerful EM simulation environment, anthropomorphic phantoms, tissue electrical properties and a measurement system. The simulation tool provides ease in modelling and accurate numerical analysis. The measurement system reduces to the antenna system around the organ of interest. Tissue mimicking properties help to understand the wave propagation through the human organ. Realistic human-like phantoms are crucial to understanding the complex structure of the organ with defined electrical properties. Modelling complex phantoms is the decisive factor for the accuracy and validation of the imaging scenario. Voxel and STL formats are widely available for designing phantoms [6]. The source format of the phantom is highly complex and requires efficient strategies to reduce the complexity of the structure while retaining accuracy.

The proposed study is focused on the study and accurate design of voxel based anatomically realistic head phantom for MWI purposes. The phantom data is usually derived from MRI images. The model is obtained from an online repository [7] in binary format. The 3D EM simulation platform WIPL-D Pro helps to transform the medical data into the 3D electromagnetic head model [8]. The unit structure of the actual phantom is a voxel or small cube with a side length of approximately 1 mm. The source file contains around 4 million such voxels. Each voxel has its own defined tissue properties. Simulation of such a model is very challenging. Therefore, with efficient procedures, the complexity is reduced. The voxels are grouped to form a big cube and then homogenization techniques are implemented on these big cubes. As mentioned, each voxel defined with one cube leads to a huge requirement of resources, therefore at the initial stage voxels are grouped using the parameter N, where N denotes the total number of voxels along each axis. The reference model is created with N=3. The homogenization is implemented using various mixing formulas [9]. A group of voxels with the given value of N is treated as one big cube, and its electrical property is derived from the averaging techniques. Implementing these methods significantly reduces the computational requirement and speeds up the simulation for EM analysis within the measurement system. In order to study the agreement between homogenization techniques and reduction in complexity, EM simulation is performed for various values of N ranging from 3 to 12 voxels in each axis. The excitation is a plane wave for the bistatic RCS estimation. The deviation between the reference model and the model with higher values of N gives the information on the accuracy of the simplification process in terms of % error. At the same time, the Relative Mean Absolute (RMA) differences between the reference model and other models (with N>3) give insight in the averaging process and its convergence.

The paper is divided into three main sections. Section II is about the voxel model and homogenization techniques,

Mladjen Stevanetic is with WIPL-D d.o.o. Belgrade, Serbia (e-mail: mladjen.stevanetic@wipl-d.com)

Branko Kolundzija is with WIPL-D d.o.o. Belgrade, Serbia and School of Electrical Engineering, University of Belgrade, Serbia (e-mail: branko.kolundzija@wipl-d.com).

Tushar Singh is with WIPL-D d.o.o. Belgrade, Serbia and School of Electrical Engineering, University of Belgrade, Serbia (e-mail: tushar.singh@wipl-d.com).

Marija Nikolic Stevanovic is with School of Electrical Engineering, University of Belgrade, Serbia (e-mail: mnikolic@etf.bg.ac.rs).

Section III is focused on numerical results, and Section IV concludes the paper.

II. Voxel Phantom and Homogenization

A. Voxel phantom

The voxel phantom represents dispersive dielectric properties data of a part of the human body (organ(s)), as a result of the MRI (Magnetic Resonance Imaging) or CT (computed tomography x-ray) scans of respective human body part [7].

That scan outputs the grid of points, named voxels, distributed in three-dimensional volume that covers the scanned organ with a specific resolution. Each voxel brings different dielectric properties of tissue. Although some phantom use Cole-Cole and Debye parameters to present dielectric properties of the tissue [10] - [11], this type of phantom comes with the binary input that holds identifications of tissue types for each voxel. The number of voxels varies depending on organ size and scanning resolution from 2 to 20 million or more. The resolution or distance between voxels is considered around 0.5 mm or 1 mm. Some of the voxels contain information on the surrounding media, in our case it is air.

However, it is very challenging and still under research to simulate the entire model with millions of unknowns, defined with thousands of domains i.e., closed regions with the same dielectric properties. Today's most robust full MoM solver, WIPL-D, reinforced with the HOBFs and fully parallelized, still requires large simulation time for millions of unknowns. Therefore, we designed a simple procedure, built-in WIPL-D, for transforming the medical data to the electromagnetic model being simulated in a reasonable amount of time and providing valuable information for overall phantom analysis.

B. Homogenization

All the voxels are treated as small cubic volumes in space with specific dielectric constant values. Generally, these values are different for different voxels but are similar for the voxels of the same tissue type. In order to decrease the complexity of such a significant problem, we perform the averaging techniques on voxels. We create bigger cubic volumes that contain several voxels, taking the same number of voxels per each of the coordinate axes of a new, larger volume. If we treat one voxel as a small cube with a size equal to the resolution of the phantom, we create a big cube with N voxels per axis. Fig. 1 shows a preview of the Zubal head phantom [7] in two resolutions $N=3$ and $N=8$ on the WIPL-D Pro platform.
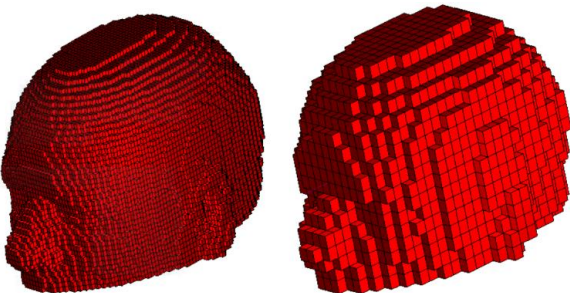

Fig. 1. Zubal anthropomorphic head phantom. Left, resolution $N=3$ and right, resolution $N=8$.

By increasing N, the resolution and therefore the complexity is gradually decreased, but the error due to averaging procedure is increased.

The new, big cube, represents a building element of the electromagnetic model. Its effective permittivity is obtained using mixing or averaging formulas applied to all the dielectric constant values of the voxels inside the same cube. These formulas were initially implemented for physical mixtures.

Standard averaging formula implements standard arithmetic mean:

$$\varepsilon_{eff} = \frac{\sum_{i=1}^{N^3} v_i * \varepsilon_i}{\sum_{i=1}^{N^3} v_i}, \qquad (1)$$

where ε_i is voxel dielectric constant and v_i is voxel volume.

Lichtenecker formula is a logarithmic formulation of physical components of the mixture as shown below:

$$\ln(\varepsilon_{eff}) = \frac{\sum_{i=1}^{N^3} v_i * \ln(\varepsilon_i)}{\sum_{i=1}^{N^3} v_i}. \qquad (2)$$

The formula has been established for biological materials such as human blood [12].

Looyenga equation is considered to be the most reliable formulation to predict the effective permittivity of the mixture [13] - [14]:

$$\varepsilon_{eff}^{\left(\frac{1}{M}\right)} = \frac{\sum_{i=1}^{N^3} v_i * \varepsilon_i^{\left(\frac{1}{M}\right)}}{\sum_{i=1}^{N^3} v_i}, \qquad (3)$$

where $M = 2, 3$. Looyenga equation is considered up to third degree. All the formulas were implemented and the results of conversion of the phantom to the electromagnetic model as well as simulated results, and its comparison, were provided for each of the formulas. That is given in the next section.

Once the effective dielectric constant that represents averaged value of all the voxels permittivity inside a big cube is obtained, the second level of homogenization is applied. It implies all the big cubes being considered to define a finite number of the domains. Hence the number of big cubes is still significant, for example, more than 100000 in some cases, each cube cannot represent a separate domain. Therefore, all the cubes are divided into several groups, where, inside each group, a relative deviation of the effective dielectric constant is kept below some small threshold. In other words, the cubes in the group possess similar values of effective dielectric constant. One group defines one domain. The domain dielectric constant is a mean value of all effective dielectric constants within the group. The domain dielectric constant is assigned to all the cubes in the group as their new averaged value (new effective dielectric constant) because it is used in the electromagnetic simulation of the phantom. We called it "the assigned dielectric constant".

The number of the domains approximately goes from 100 to 300 for all the resolutions and all four mixing formulas considered in the paper. The higher the resolution (lower N)

the number of domains generally decreasing and approaches to the number of different tissue types in the model. Each domain represents a closed region, and all the mesh elements, or big cubes' sides, inside the domain were removed to reduce complexity and thus the number of unknowns in the final model. Only domains' surface mesh elements took part in the MoM simulation.

The last part of big cubes' creation is the calculation of the deviation. For each cube, the deviation is calculated per the above-mentioned formulas. The formula used for averaging is also used for calculating deviation. The only difference is that part ε_i in the above equations is changed with the $|\varepsilon_i - \varepsilon'_{eff}|$ which is the deviation of one small voxel. Therefore, the Lichtenecker method is given as

$$\ln(\delta) = \frac{\sum_{i=1}^{N^3} v_i * \ln |\varepsilon_i - \varepsilon'_{eff}|}{\sum_{i=1}^{N^3} v_i}, \quad (4)$$

standard and Looyenga method is

$$\delta^{\left(\frac{1}{M}\right)} = \frac{\sum_{i=1}^{N^3} v_i * |\varepsilon_i - \varepsilon'_{eff}|^{\left(\frac{1}{M}\right)}}{\sum_{i=1}^{N^3} v_i}, \quad (5)$$

where $M = 1, 2, 3$, v_i is voxel volume and ε'_{eff} is the assigned dielectric constant value.

Therefore, a mean deviation for each big cube is calculated as the mean absolute distance of each voxel in the cube from the assigned dielectric constant value, rather than the distance from the averaged value ε_{eff}.

C. Estimation of Error

In the end, the deviation for the whole phantom is obtained from the particular deviations of big cubes. This value actually represents the error raised from the averaging procedure.

The error value is also calculated using a specific formula which is similar to the averaging process, so, either with standard, Lichtenecker or Looyenga procedure. Lichtenecker method

$$\ln(\Delta) = \frac{\sum_{j=1}^{K} V_j * \ln(\delta_j)}{\sum_{j=1}^{K} V_j}, \quad (6)$$

standard and Looyenga method

$$\Delta^{\left(\frac{1}{M}\right)} = \frac{\sum_{j=1}^{K} V_j * \delta_j^{\left(\frac{1}{M}\right)}}{\sum_{j=1}^{K} V_j}, \quad (7)$$

where K is number of big cubes, $M = 1, 2, 3$, δ_j is the big cube deviation and V_j is big cube volume. We can calculate the average value A of the whole phantom using the Lichtenecker method

$$\ln(A) = \frac{\sum_{j=1}^{K} \sum_{i=1}^{N^3} v_{ji} * \ln |\varepsilon_{ji}|}{\sum_{j=1}^{K} \sum_{i=1}^{N^3} v_{ji}}, \quad (8)$$

standard and Looyenga method

$$A^{\left(\frac{1}{M}\right)} = \frac{\sum_{j=1}^{K} \sum_{i=1}^{N^3} v_{ji} * |\varepsilon_{ji}|^{\left(\frac{1}{M}\right)}}{\sum_{j=1}^{K} \sum_{i=1}^{N^3} v_{ji}}, \quad (9)$$

where K is number of big cubes, $M = 1, 2, 3$, v_{ji} is voxel volume of i-th voxel in the j-th big cube and ε_{ji} is voxel dielectric constant of i-th voxel in the j-th big cube. The air voxels are omitted from the overall phantom.

Now, we can calculate the relative mean absolute error of the whole phantom as

$$RMA[\%] = \frac{\Delta}{A} * 100. \quad (10)$$

This value is provided at the end of the conversion process of the phantom to the electromagnetic model, ready for simulation.

The relative mean absolute deviation of simulated results is given by

$$RMA_{sim}[\%] = \frac{\frac{1}{n} * \sum_{i=1}^{n} |E_i^N - E_i^{Ref}|}{\frac{1}{n} * \sum_{i=1}^{n} |E_i^{Ref}|} * 100, \quad (11)$$

where n is the number of directions for bistatic RCS far-field, here 73x37 for azimuth and elevation, E_i^N is far-field for phantom with resolution N and E_i^{Ref} is far-field for the reference fantom.

III. RESULTS

We used the Zubal head phantom for analysis. The full MoM electromagnetic simulations were performed in WIPL-D software.

Simulations in WIPL-D provide results for bistatic RCS in a number of space angles, with plane wave excitation. The results were provided for different resolutions *N*=3, 4… 12 and for all mixing formulas, Lichtenecker and Looyenga where *M*=1, 2, 3. We also provide the *RMA* values for all the conversions.

The phantom with the highest resolution, *N*=3, is taken as the reference result. At the operating frequency of 1 GHz, this phantom has 500000 unknowns with around 100 domains and the resolution is about 3.5 mm. Simulation time on the machine Intel(R) Xeon(R) CPU E5-2650 v4 @ 2.20GHz (2 processors), with 48 logical processors, 256 GB of RAM and 4 GPU cards NVIDIA GeForce GTX 1080Ti, is about 7.3 hours.

All other phantoms were compared to this reference phantom, mean deviation of the RCS far-field is calculated for each of them relative to the reference phantom i.e., *RMA_sim*. In the same manner, the differences were provided for the *RMA* values too, relative to the reference phantom.

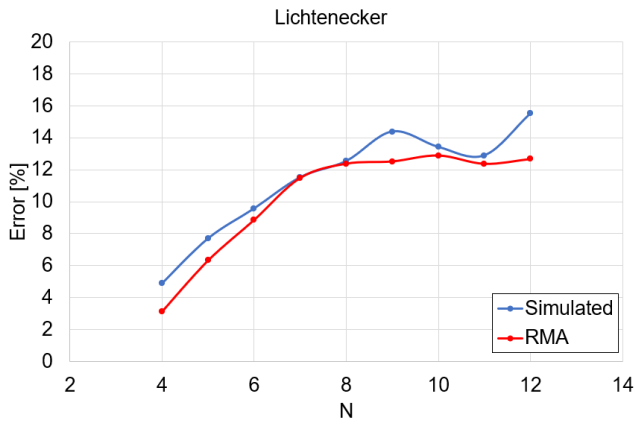The next four figures present a comparison of *RMA_sim* and *RMA* relative to the reference phantom.

Fig. 2. Lichtenecker method. The Error for the blue trace represents the mean deviation of the RCS far-field relative to the reference phantom N=3 i.e., RMA_{sim}. The Error for the red trace represents differences in RMA also relative to the reference phantom N=3. N is resolution.
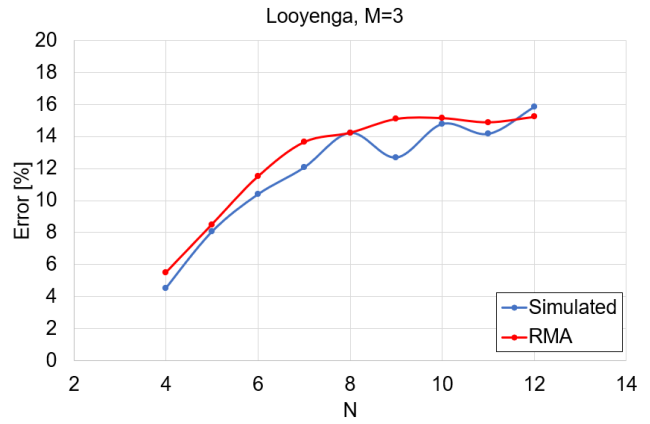

Fig. 3 Looyenga method, with M=1 degree. The Error for the blue trace represents the mean deviation of the RCS far-field relative to the reference phantom N=3 i.e., RMA_{sim}. The Error for the red trace represents differences in RMA also relative to the reference phantom N=3. N is resolution.
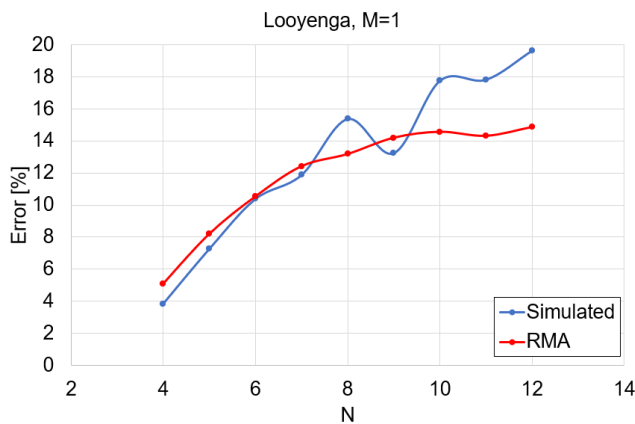

Fig. 4. Looyenga method, with M=2 degree. The Error for the blue trace represents the mean deviation of the RCS far-field relative to the reference phantom N=3 i.e., RMA_{sim}. The Error for the red trace represents differences in RMA also relative to the reference phantom N=3. N is resolution.
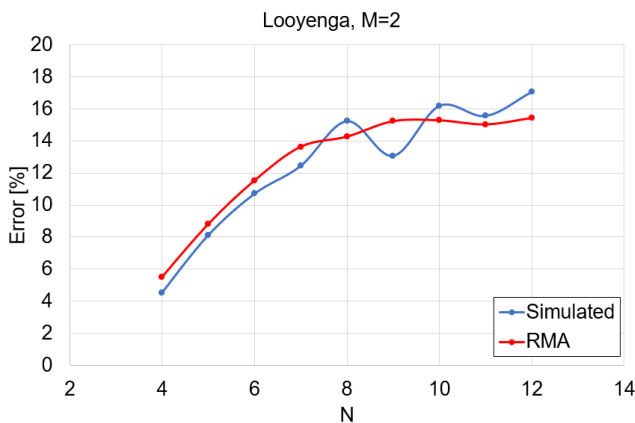

Fig. 5. Looyenga method, with M=3 degree. The Error for the blue trace represents the mean deviation of the RCS far-field relative to the reference phantom N=3 i.e., RMA_{sim}. The Error for the red trace represents differences in RMA also relative to the reference phantom N=3. N is resolution.

IV. CONCLUSION

We present a novel technique for the conversion of large voxel phantoms by averaging and homogenization of the voxel data to the electromagnetic simulation ready model. The obtained model is suitable for analysis of the imaging scenario, with reasonable simulation time.

We've also shown the estimated error, or relative mean absolute value RMA, as a result of the simplification process. A comparison in error behavior between RMA and simulated RCS results is provided. It can be seen that the RMA expresses very similar behavior with the mean deviation in simulated results, for different resolutions, relative to some phantom of a very high resolution taken as the reference. The estimated convergence of the RMA can serve as a guide of anticipating the characteristics of the phantom before performing electromagnetic simulation itself.

REFERENCES

[1] S. Mustafa, B. Mohammed and A. Abbosh, "Novel Preprocessing Techniques for Accurate Microwave Imaging of Human Brain," in IEEE Antennas and Wireless Propagation Letters, vol. 12, pp. 460-463, 2013

[2] A.S. M. Alqadami, A. Trakic, A. E. Stancombe, B. Mohammed, K. Bialkowski and A. Abbosh, "Flexible Electromagnetic Cap for Head Imaging," in IEEE Transactions on Biomedical Circuits and Systems, vol. 14, no. 5, pp. 1097-1107, Oct. 2020, doi: 10.1109/TBCAS.2020.3025341.

[3] Zhao Wang, Eng Gee Lim, Yujun Tang, Mark Leach, "Medical Applications of Microwave Imaging", The Scientific World Journal, vol. 2014, Article ID 147016, 7 pages, 2014. https://doi.org/10.1155/2014/147016.

[4] M. Pastorino, A. Randazzo, Microwave Imaging Methods and Applications, in *Artech House*, 2018.

[5] L. Crocco, I. Karanasiou, M. James, R. Conceição, "Emerging Electromagnetic Technologies for Brain Diseases Diagnostics, Monitoring and Therapy," *Springer*, Cham, Switzerland, 2018.

[6] S. N. Makarov, G. M. Noetscher and A. Nazarian, Low-Frequency Electromagnetic Modeling for Electrical and Biological Systems Using Matlab, *John Wiley & Sons*, Inc, 2016

[7] The Zubal Phantom – http://noodle.med.yale.edu/zubal/

[8] WIPL-D software suite (WIPL-D Pro v17 & Pro CAD 2020), WIPL-D d.o.o, Belgrade, 2020.

[9] T. Singh, M. Stevanetic, M. Stevanovic and B. Kolundzija, "Homogenization of Voxel Models using Material Mixing Formulas," 2020 14th European Conference on Antennas and Propagation (EuCAP), 2020, pp. 1-4.

[10] Zastrow E, Davis SK, Lazebnik M, F. Kelcz, B. D. Van Veen, and S. C. Hagness, Database of 3D grid-based numerical breast phantoms for

use in computational electromagnetics simulations. Madison (WI): University of Wisconsin-Madison; c2014. [cited 2014 Sep 21]. Available at: https://uwcem.ece.wisc.edu/phantomRepository.html.

[11] M. Lazebnik, L. McCartney, D. Popovic, C. B. Watkins, M. J. Lindstrom, J. Harter, S. Sewall, A. Magliocco, J. H. Booske, M. Okoniewski, and S. C. Hagness, "A large-scale study of the ultrawideband microwave dielectric properties of normal breast tissue obtained from reduction surgeries," Physics in Medicine and Biology, vol. 52, pp. 2637-2656, April 2007.

[12] Ray Simpkin, "Derivation of Lichtenecker's Logarithmic Mixture Formula From Maxwell's Equations," IEEE Transactions on Microwave Theory and Techniques, Vol. 58, No. 3, March 2010.

[13] S.O. Nelson, "Measurement and Computation of Powdered Mixture Permittivities," Proceedings of the 17th IEEE Instrumentation and Measurement Technology Conference, DOI: 10.1109/IMTC.2000.848661.

[14] Kimmo Kalervo Kärkkäinen, Ari Henrik Sihvola, and Keijo I. Nikoskinen, "Effective Permittivity of Mixtures: Numerical Validation by the FDTD Method," IEEE Transactions on Geoscience and Remote Sensing, Vol. 38, No. 3, May 2000 1303.